(Preprint) AAS 15-201

MARS DOUBLE-FLYBY FREE RETURNS

Mark Jesick*

A subset of Earth-originating Mars double-flyby ballistic trajectories is documented. The subset consists of those trajectories that, after the first Mars flyby, perform a half-revolution transfer with Mars before returning to Earth. This class of free returns is useful for both human and robotic Mars missions because of its low geocentric energy at departure and arrival, and because of its extended stay time in the vicinity of Mars. Ballistic opportunities are documented over Earth departure dates ranging from 2015 through 2100. The mission is viable over three or four consecutive Mars synodic periods and unavailable for the next four, with the pattern repeating approximately every 15 years. Over the remainder of the century, a minimum Earth departure hyperbolic excess speed of 3.16 km/s, a minimum Earth atmospheric entry speed of 11.47 km/s, and a minimum flight time of 904 days are observed. The algorithm used to construct these trajectories is presented along with several examples.

INTRODUCTION

With water ice, an Earth-like day, a carbon dioxide atmosphere, and its proximity to Earth, Mars is an enticing destination for human exploration and colonization. The Red Planet is also an exciting scientific target as it potentially offers an environment for past or present indigenous life. To date, Mars has been successfully visited by over 20† robotic spacecraft that have made key discoveries about its surface and atmospheric composition as well as discoveries about the existence of liquid water in its past. However, no human or robotic round-trip mission to Mars has yet been accomplished, in spite of continued interest. The double-flyby free return is proposed as an effective method of carrying out such missions.

A Mars double-flyby free return departs Earth, performs a flyby of Mars, performs a second Mars flyby on the opposite side of the sun, and returns to Earth (Fig. 1). A human mission following such a trajectory was first suggested by Zubrin in 1996 as a cost-effective first step in a Mars exploration program to prove that human flights to Mars are feasible with modest technology advancements, and do not present prohibitive risk.[1] A trajectory of this class offers Earth departure and return energies comparable to conjunction-class missions,[2] and a direct reentry speed at Earth as little as 4% greater than Apollo values.[3] The double-flyby free return always remains at least one astronomical unit from the sun, and provides an extended stay time of about 300 days in near-Mars space. The downside of the double-flyby mission is that the typical flight time is between 900 and 1000 days (this, however, is equivalent in duration to a typical conjunction-class surface mission).

*Navigation Engineer, Inner Planet Navigation Group, Jet Propulsion Laboratory, California Institute of Technology, 4800 Oak Grove Drive, Pasadena, California 91109; jesick@jpl.nasa.gov. Member AIAA.

†Data available at `http://nssdc.gsfc.nasa.gov/planetary/chronology_mars.html` [accessed 10 October 2014]

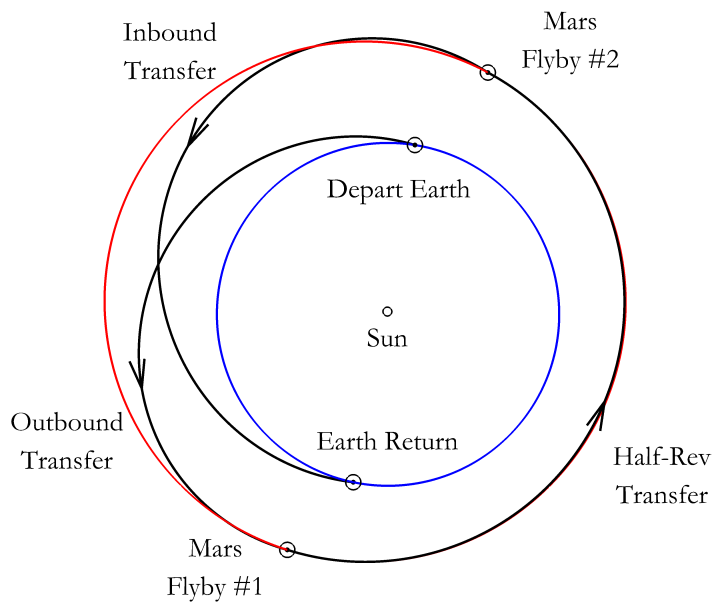

Figure 1. Mars double-flyby free return.

Beyond the human flyby mission (which will be discussed below in more detail), the double-flyby free return has other potential applications for human, robotic, and combined human/robotic missions. First, the double-flyby could be used for a human mission to the surface of Mars. In this scenario, near the first hyperbolic passage, an entry vehicle with crew separates from the on-orbit habitat, enters the atmosphere, descends, and lands. The orbital habitat, containing systems essential in deep space but too massive to be easily transported to the ground, performs the first flyby and remains on the half-revolution transfer (also called a "π transfer") for half a Martian year while the crew explore the surface. As the orbital habitat approaches Mars for the second flyby, the crew ascend from the surface and perform a hyperbolic rendezvous with the habitat for the return voyage to Earth. (This is similar in concept to the flyby-landing excursion mode proposed by Titus.[4]) This scenario's timeline is comparable to that of a conjunction-class mission; the advantage here is that the entire mass of the transport infrastructure does not need to perform propulsive maneuvers to enter and leave Mars orbit. A similar strategy could be followed for human exploration of Phobos and Deimos. Second, the double-flyby trajectory is also useful for telerobotic operations on the surface of Mars or its moons. In this case, an uncrewed vehicle separates form the crewed orbital habitat and either descends to the Martian surface or to Phobos or Deimos. During the half-revolution transfer, the crew remain within one light minute of Mars for hundreds of days. Incorporating the ability to operate robotic surface assets at this distance increases the scientific value of such a mission. This mission profile is also well suited for crewed sample return since the uncrewed vehicle can rendezvous with the returning orbital habitat during the second Mars flyby. Third, the double-flyby can be used for robotic sample return. In a surface sample return mission, a sample retrieval vehicle separates from the Earth reentry infrastructure which remains in heliocentric orbit. The retrieval vehicle descends to the Martian surface or to Phobos or Deimos and has about 300 days to locate and cache samples. During the next hyperbolic passage of the orbital vehicle, the two vehicles meet and make the return journey to Earth. An alternate to the surface sample return mission is the atmo-

Table 1. Potential applications for Mars double-flyby free returns

Mission	Description
Human flyby	Crewed spacecraft performs two Mars flybys and returns to Earth.
Human surface exploration	Crewed vehicle separates from orbital spacecraft and descends to Mars' surface for approximately 300 days. Crew ascend, perform rendezvous with orbital vehicle on its second Mars flyby, and return to Earth.
Human Phobos/Deimos exploration	Crewed vehicle separates from orbital spacecraft to rendezvous with Phobos and/or Deimos. After about 300 days, crew perform rendezvous with orbital vehicle on its second Mars flyby, and return to Earth.
Telerobotic surface exploration (with potential sample return)	Robotic vehicle separates from orbital spacecraft and descends to Mars' surface. Crew remain in orbital vehicle and teleoperate robotic surface vehicle. Crew perform second Mars flyby and return to Earth. Can also be performed with existing or pre-deployed Mars surface assets. For sample return option, robotic vehicle ascends and performs hyperbolic rendezvous during the second Mars flyby. Alternatively, crew could enter low Mars orbit while Earth reentry infrastructure remains on free return.
Telerobotic Phobos/Deimos exploration (with potential sample return)	Robotic vehicle separates from orbital spacecraft to rendezvous with Phobos and/or Deimos. Crew remain in orbital vehicle and teleoperate robotic vehicle. Crew perform second Mars flyby and return to Earth. For sample return option, robotic vehicle performs hyperbolic rendezvous during the second Mars flyby. Alternatively, crew could enter low Mars orbit while Earth reentry infrastructure remains on free return.
Robotic surface sample return	Robotic vehicle separates from orbital spacecraft and descends to Mars' surface for approximately 300 days, collecting surface samples. Vehicle ascends, performs rendezvous with orbital spacecraft on its second Mars flyby, and returns to Earth.
Robotic Phobos/Deimos sample return	Robotic vehicle separates from orbital spacecraft to rendezvous with Phobos and/or Deimos, collecting samples. After about 300 days, the vehicle ascends, meets the orbital spacecraft on its second Mars flyby, and returns to Earth.
Robotic atmosphere sample return	Robotic spacecraft performs two Mars flybys, collecting atmospheric samples at different locations at different epochs, and returns samples to Earth. Alternatively, sampling could be performed by vehicle in low Mars orbit while Earth reentry infrastructure remains on free return.

spheric sample return mission where a vehicle dips through the Martian atmosphere at each passage. Thus, two samples are gathered at unique epochs and atmospheric locations. Table 1 summarizes potential applications for the double-flyby free return.

Much research has been performed on ballistic return trajectories that pass Mars, but these works focus mainly on single flybys. Previously, Wolf presented Mars free-return trajectories with an optional Venus flyby on the outbound and/or inbound legs during the launch period 2000–2020.[5] Patel, Longuski, and Sims documented Mars single-flyby free return opportunities from 1995 to 2020 in an ephemeris model with zero sphere of influence dynamics.[6] The study showed that two- and three-year duration free return opportunities occur each Earth-Mars synodic period. Of great interest were the free returns with a flight time of approximately 1.4 years. The analysis showed that launch opportunities for these "fast" free returns are available only twice every fifteen years. (This class actually repeats synodically also, but the departure energy during the other opportunities is greater than the maximum value considered in that study.) Crain, Bishop, Fowler, and Rock used

a global search method in combination with a local search routine to seek ballistic and near-ballistic Mars flyby opportunities.[7] The use of a genetic algorithm enabled exploration of the solution space without requiring the computational effort of a broad grid search. One noteworthy outcome of this study was the documentation of a near-ballistic Mars flyby opportunity of less than one year in round-trip flight time; the drawback is that this trajectory requires departure and return hyperbolic excess velocities at Earth greater than 12 km/s. Bonfiglio, Longuski, and Vinh extended previous work to include the effect of atmospheric passage during the Mars flyby and an optional Venus flyby.[8] This aerogravity-assist technique was found to significantly reduce the Earth departure and return energy in some cases. Okutsu and Longuski document additional free return opportunities that incorporate a Venusian gravity assist.[9]

A related topic receiving much attention is Earth-Mars cyclers. The Mars double-flyby free return is similar in some respects to the cycler concept since an Earth-Mars cycler is a periodic ballistic (or nearly ballistic) trajectory which connects Earth and Mars.[10–13] The double-flyby trajectory allows, like cyclers, on-orbit infrastructure to remain in heliocentric orbit and provides multiple encounters with Earth and Mars. Though the double-flyby is not repeatable, it offers lower energy at the encounters than known cyclers.

In contrast to previous studies, the present work is unique because it specifically investigates the Earth-Mars-Mars-Earth free return profile. The main purpose here is to document all double-flyby free returns for the remainder of the century. Additionally, the method used to generate these trajectories is presented. Before the algorithms and results are described, however, the human flyby mission is discussed in more detail.

Human Double-Flyby Mission

A subject that warrants further discussion is human flight to the Martian vicinity and, in particular, how it can be facilitated by the double-flyby free return. A seminal study of a crewed mission to the Red Planet was *The Mars Project* in the early 1950s.[14] Since that time, much work has been done on the subject.[4,15–21] A round-trip mission to the Martian surface, however, poses the problem of descending and ascending with crew and supplies through Mars' atmosphere. To date, the largest payload delivered to the surface was the 900 kg Mars Science Laboratory,[22] but a human mission may require ten times this amount.[‡] In addition, humanity has no experience in the return voyage from the Martian surface to Earth. These challenges inevitably add to the complexity and cost of such a mission. To circumvent these difficulties, some have proposed a flyby mission as a potential first step.[1,23–27]

A Mars flyby mission would transport crew from Earth, perform a flyby of Mars without capturing or landing, and return to Earth. Perhaps most important, a Mars flyby mission would achieve a number of firsts: the first human interplanetary voyage, and the first human flyby of Mars. Such a mission is questionable on purely scientific grounds, but it necessitates the development of technologies that can subsequently enable broader science through expanded human exploration. Also, a crewed Mars flyby mission, though not enabling human excursions on the Martian surface, provides deep space operational experience in dealing with solar and cosmic radiation, developing life support systems longevity, and measuring psychological effects of long-duration spaceflight beyond low Earth orbit. A successful flyby mission also validates technology for in-space propulsion and habitats to be used for subsequent missions. Just as Apollo 7 and 9 were missions to low Earth

[‡]For comparison, each lunar lander to reach the surface of the moon had an initial mass of at least 15000 kg.[3]

orbit, and Apollo 8 and 10 were lunar orbiting missions with no landing component, the Mars flyby mission would be a stepping stone to the ultimate goal of a human landing on the Red Planet.

In many ways, the flyby mission is less difficult than a crewed mission to the surface or even to a closed Martian orbit. The flyby mission requires no propulsive architecture for Mars orbit insertion or trans-Earth injection, and provides crew a maneuver-free ballistic return, albeit after a flight of hundreds of days. Additionally, there is no need for human-scale entry, descent, and landing technology development and implementation. There is no need for long-duration surface systems, which may need to operate on the Martian surface from tens to hundreds of days, depending on the mission type. Each system necessitates an increased mass at Earth departure, and, therefore, increased launch vehicle capability above what a flyby mission would require. However, the flyby mission is actually more challenging in other aspects. A main concern for crew during a flyby mission is continuous exposure to microgravity and increased radiation, resulting in bone-mass loss, increased risk of cancer, and other problems; a landing would offer a respite from these effects with a 3/8 Earth gravity environment and some radiation shielding.[28] One potential way to counter the effects of microgravity during a flyby mission is to employ "artificial gravity" whereby the spacecraft is spun up to produce a centripetal acceleration. Such a concept is worth noting here but is not within the scope of this study.

Because of the health risks posed by long duration spaceflight, round-trip flight time is an important concern in the design of Mars flyby missions.[§] However, the Mars free return trajectories which offer the shortest flight time also require the highest energy at Earth departure and return, in general. The fastest Earth atmospheric reentry speed of a spacecraft was 12.799 km/s on the Stardust mission, and that was to return a capsule of 46 kg.[29] The fastest reentry of a human vehicle was 11.069 km/s on Apollo 10.[3] Single-flyby Mars free returns with a flight time of about 1.5 years, for example, require a hyperbolic excess velocity at Earth departure of 6 km/s or greater, and entail a direct atmospheric reentry speed of 14 km/s or more, which is nearly a 30% increase over the maximum Apollo value. Such a reentry speed requires either significant advancements in thermal protection system technology, a propulsive braking maneuver, or the execution of aerobraking maneuvers to split the task of energy decrease across multiple atmospheric passes.

Use of the Mars double-flyby free return eliminates some of the problems associated with single-flyby free returns. A trajectory of this class offers reduced energy at Earth departure and arrival, and an extended stay in near-Mars space relative to fast (1.5 yr) single-flyby free returns. The Earth departure energy can be 40–50% less than the fast free return trajectories. Also, the double-flyby free return always remains at least one astronomical unit from the sun whereas fast free returns generally require the spacecraft to travel near or inside Venus' orbit, thus exposing crew to a heightened solar radiation environment. The downside of the double-flyby mission is that the typical flight time is about 910 days. Thus, the flight time of the double-flyby free return is less advantageous when compared to the fast free returns, but the double-flyby is superior in terms of Earth departure and return energy, and time spent in near-Mars space.

SOLUTION METHOD

A zero sphere of influence patched conic model is used for spacecraft dynamics. During interplanetary cruise, the sun's gravity alone acts on the spacecraft, and each heliocentric trajectory

[§]The current record for cumulative time in space is held by Sergei Krikalev at 803 days. See `http://www.jsc.nasa.gov/Bios/htmlbios/krikalev.html` [accessed 3 July 2014].

segment begins and terminates at the center of a massless Earth or Mars. During a hyperbolic planetary encounter, the spacecraft is influenced by that body's gravity only. Planetary positions are taken from JPL's DE405 ephemeris with the SPICE toolkit.[30] Therefore, the spacecraft's trajectory is conic in each regime, but the planetary trajectories are not.

Flyby Construction

When modeling planetary encounters, a powered flyby methodology is used in which the spacecraft performs a propulsive maneuver before or after the encounter.[13] This method captures ballistic opportunities (where no flyby maneuver is necessary) as well as near-ballistic opportunities (where the flyby maneuver is small). All powered flybys are performed at the edge of the flyby planet's sphere of influence, either before or after the flyby depending on the magnitudes of the incoming and outgoing $\boldsymbol{v}_\infty$ vectors. The minimum flyby altitude at Mars is 200 km.

Given an incoming and outgoing hyperbolic excess velocity at a body, denoted here as $\boldsymbol{v}_\infty^-$ and $\boldsymbol{v}_\infty^+$, respectively, a maneuver is performed at the edge of the sphere of influence to produce a feasible flyby which satisfies the minimum altitude constraint. The flyby and maneuver occur in the plane containing the $\boldsymbol{v}_\infty$ vectors. The maximum available turning angle across the flyby is $\delta_{avail} = \max(\delta^+, \delta^-)$ where

$$\delta^\pm = 2 \arcsin \left[\left(1 + \frac{r_{p_{min}} v_\infty^\pm}{\mu} \right)^{-1} \right] \tag{1}$$

where δ^+ is the turning angle based on v_∞^+, δ^- is the turning angle based on v_∞^-, $r_{p_{min}}$ is the minimum allowed flyby periapsis radius, and μ is the flyby body's gravitational parameter. The required turning angle is

$$\delta_{req} = \arccos \left(\frac{\boldsymbol{v}_\infty^{-\top} \boldsymbol{v}_\infty^+}{v_\infty^- v_\infty^+} \right) \tag{2}$$

The actual turning angle is chosen to be

$$\delta = \min(\delta_{req}, \delta_{avail}) \tag{3}$$

If $v_\infty^- \leqslant v_\infty^+$, the maneuver is performed after the flyby (Fig. 2(b)). The post-flyby velocity achieved through the ballistic flyby is

$$\boldsymbol{v}_\infty^{+-} = v_\infty^- \cos\delta \; \hat{\boldsymbol{v}}_\infty^- + v_\infty^- \sin\delta \; \hat{\boldsymbol{h}} \times \hat{\boldsymbol{v}}_\infty^- \tag{4}$$

where

$$\hat{\boldsymbol{h}} = \frac{\boldsymbol{v}_\infty^- \times \boldsymbol{v}_\infty^+}{|\boldsymbol{v}_\infty^- \times \boldsymbol{v}_\infty^+|} \tag{5}$$

To account for the difference between this velocity and the required post-flyby velocity, $\boldsymbol{v}_\infty^+$, the post-flyby maneuver is applied:

$$\Delta \boldsymbol{v} = \boldsymbol{v}_\infty^+ - \boldsymbol{v}_\infty^{+-} \tag{6}$$

If $v_\infty^- > v_\infty^+$, the maneuver is performed before the flyby (Fig. 2(a)). The pre-flyby velocity that achieves $\boldsymbol{v}_\infty^+$ after the ballistic flyby is

$$\boldsymbol{v}_\infty^{-+} = v_\infty^+ \cos\delta \; \hat{\boldsymbol{v}}_\infty^+ + v_\infty^+ \sin\delta \; \hat{\boldsymbol{h}} \times \hat{\boldsymbol{v}}_\infty^+ \tag{7}$$

To account for the difference between this velocity and the required pre-flyby velocity, $\boldsymbol{v}_\infty^-$, the pre-flyby maneuver is applied:

$$\Delta \boldsymbol{v} = \boldsymbol{v}_\infty^{-+} - \boldsymbol{v}_\infty^- \tag{8}$$

Whether the maneuver is performed before or after flyby, its magnitude is

$$\Delta v = \begin{cases} |v_\infty^+ - v_\infty^-| & \text{if } \delta_{req} \leqslant \delta_{avail} \\ \sqrt{(v_\infty^+)^2 + (v_\infty^-)^2 - 2v_\infty^+ v_\infty^- \cos(\delta_{req} - \delta_{avail})} & \text{if } \delta_{req} > \delta_{avail} \end{cases} \tag{9}$$

Alternatively, it is also possible to solve for the radius at which a periapsis maneuver may be performed during the flyby. This method, however, requires iteration and may produce a subsurface trajectory; it also adds to operational risk to require a periapsis maneuver during flyby. The Δv flyby method is preferred as it offers an analytic solution and never results in a subsurface flyby. In this case, "unfavorable" flybys are simply determined by the magnitude of the flyby maneuver.

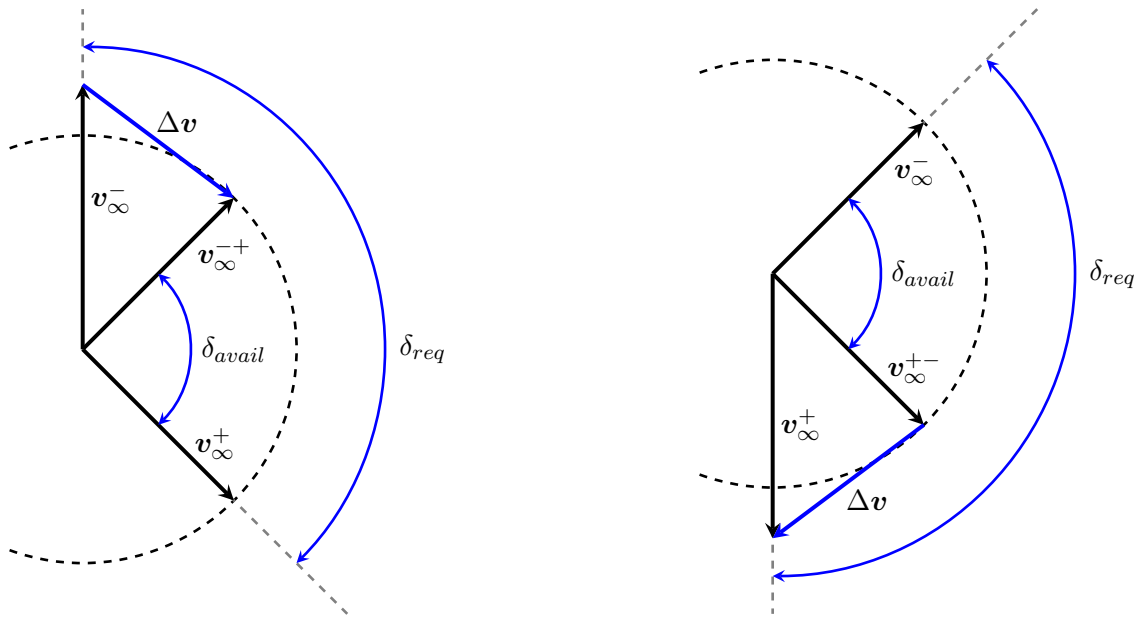

(a) Pre-flyby maneuver

(b) Post-flyby maneuver

Figure 2. Powered flyby maneuver.

Half-Revolution Transfer

To produce a half-revolution transfer after the first flyby, the spacecraft should follow an orbit given by a rotation of Mars' orbit about the sun-Mars vector $\boldsymbol{r}_{SM}$ at the flyby time t_1. This results in an orbit that intersects Mars' orbit at a position diametrically opposed to the position of the first flyby relative to the sun (assuming that both the spacecraft and Mars are under the gravitational influence of the sun only). Thus, the spacecraft's heliocentric velocity vector immediately after the first flyby is a rotation of Mars' velocity vector about the sun-Mars line at the time of the first flyby, as shown in Fig. 3. It is also possible for the spacecraft to complete the half-revolution transfer after Mars has completed $(2n-1)/2$ revolutions for $n = 2, 3, \ldots$, but this is undesirable for certain

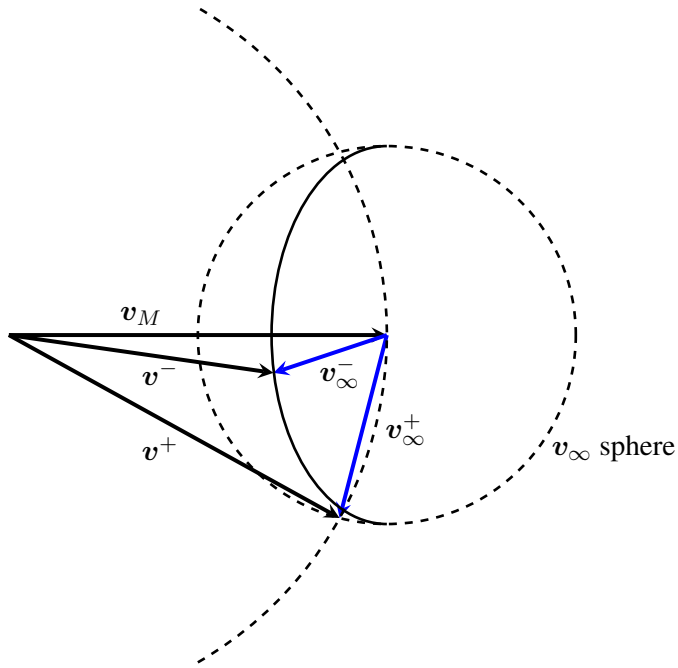

Figure 3. Half-revolution flyby velocity diagram. The heliocentric position vector of Mars is normal to the plane of the paper. The velocity $\boldsymbol{v}_M$ of Mars is, in general, not in the plane of the paper.

missions because of the increased flight time and because the spacecraft will not remain near Mars along the transfer. Such transfers are not considered here.

The spacecraft's heliocentric velocity after the first flyby is

$$\boldsymbol{v}_1^+ = \boldsymbol{R}_{SM}^\top(\theta)\boldsymbol{v}_M(t_1) \tag{10}$$

where $\boldsymbol{R}_{SM}(\theta)$ is the rotation matrix about $\boldsymbol{r}_{SM}(t_1)$. Since $v_1^+ = v_M$, the post-flyby hyperbolic excess velocity is

$$(v_\infty^+)^2 = (v_M')^2 + (v_M')^2 - 2v_M'v_M'\cos\theta \tag{11}$$

by the law of cosines, where v_M' is the velocity of Mars projected in the plane normal to $\boldsymbol{r}_{SM}$ at the flyby epoch. Solving for the rotation angle gives

$$\theta = \xi \arccos\left[1 - \tfrac{1}{2}\left(\frac{v_\infty}{v_M'}\right)^2\right] \tag{12}$$

where

$$\xi \equiv \text{sign}(\boldsymbol{h}_M^\top \boldsymbol{v}_1^-) \tag{13}$$

where $\boldsymbol{h}_M$ is the angular momentum of Mars at the flyby epoch. Thus, if the pre-flyby heliocentric velocity points north of Mars' orbital plane, the π transfer is performed above the orbital plane; otherwise, the π transfer occurs below the orbital plane.

This analysis assumed that the orbit of Mars is conic, but this assumption does not hold due primarily to perturbations from the planets. These perturbations can result in a position offset between

the spacecraft and Mars at the second flyby on the order of 10000 km. However, the conic analysis is still useful as an initial estimate for numerical targeting. Thus, a true π transfer does not exist in general because after Mars' position vector sweeps through 180 deg about its initial angular momentum vector, its initial and final position vectors will not be diametrically opposed. To circumvent Lambert algorithm problems for transfer angles near 180 deg, a separate numerical targeting problem is solved in each case to target Mars at the second flyby. A vector of free parameters is defined as

$$\boldsymbol{x}_p \equiv \begin{bmatrix} \boldsymbol{v}_1^{+\top} & t_2 \end{bmatrix}_{1\times 4}^{\top} \tag{14}$$

where $\boldsymbol{v}_1^+$ is the heliocentric velocity after the first flyby, and t_2 is the time of the second flyby. The initial values of the free parameters come from the conic π transfer approximation. A constraint vector is defined as

$$\boldsymbol{c} \equiv \begin{bmatrix} \boldsymbol{r}(t_2) - \boldsymbol{r}_M(t_2) \end{bmatrix}_{1\times 3}^{\top} \tag{15}$$

where $\boldsymbol{r}(t_2)$ and $\boldsymbol{r}_M(t_2)$ are the positions of the spacecraft and Mars at the time of the second flyby, respectively. The spacecraft position at the second flyby, $\boldsymbol{r}(t_2)$, is computed with Kepler's equation from the state immediately after the first flyby, and Mars' position at t_2 is retrieved from the ephemeris. Convergence yields a valid half-revolution transfer in the ephemeris model.

Search Algorithm Overview

To find feasible double-flyby free returns, a grid search method is used where the Earth departure date, Earth-Mars transfer duration, and Mars-Earth transfer duration are parametrically varied in a nested loop. The algorithm is outlined in Fig. 4. First, the Earth departure date is initialized. This is the epoch at which the spacecraft leaves the Earth's sphere of influence. Next, the Earth-Mars transfer duration is initialized, which defines the outbound Lambert problem. If a valid Lambert solution is achieved and it results in an Earth departure with $v_\infty < v_{\infty_{max}}$, the π transfer is targeted next. If a solution is found, the first flyby impulse, Δv_1, is computed. If $\Delta v_1 < \Delta v_{max}$, the Mars-Earth transfer duration is initialized, and the inbound Lambert problem is solved. If a valid solution is achieved, the magnitude of the second flyby maneuver, Δv_2, is calculated. If $\Delta v_1 + \Delta v_2 < \Delta v_{max}$, the trajectory is saved to file. The Mars-Earth transfer duration is then recursively incremented until its maximum value is reached. In turn, the Earth-Mars transfer duration and Earth departure epoch are incremented as shown in Fig. 4. Table 2 shows the bounds on each variable and the default stepsize for the loop variables. A one-day grid is used for the Earth departure date, Earth-Mars transfer duration, and Mars-Earth transfer duration. Minimum and maximum Earth-Mars and Mars-Earth durations of 100 and 500 days are used. Thus, over five billion permutations are considered, albeit many are pruned before complete evaluation because the first (outbound) leg or one of the flyby maneuvers is found to be unacceptable. A finer grid may be used for higher resolution scans during opportunities of interest. Experience has shown that using a finer grid locates more ballistic trajectories, but it does not expand the launch period for feasible free returns. Although free returns are not directly targeted here, free returns are a subset of the powered flyby trajectory class, i.e. a flyby trajectory with a total flyby maneuver Δv equal to zero. Because a grid search is used to generate the present database, it may be necessary to use a local search method (or a finer grid) to more precisely locate free returns if the initial search did not provide satisfactory results.

When the algorithm finds a solution that meets the criteria for a favorable free return (in this case, remaining under the limits imposed on Earth departure energy and flyby maneuver magnitude), information necessary to reproduce the trajectory along with additional useful information (such as

Table 2. Algorithm Parameters

Quantity	Lower Limit	Upper Limit	Increment
Earth departure date	January 1, 2015	December 31, 2100	1 dy
Earth-Mars transfer duration	100 dy	500 dy	1 dy
Mars-Earth transfer duration	100 dy	500 dy	1 dy
Earth departure excess speed	0	10 km/s	—
Flyby maneuver magnitude sum	0	100 m/s	—

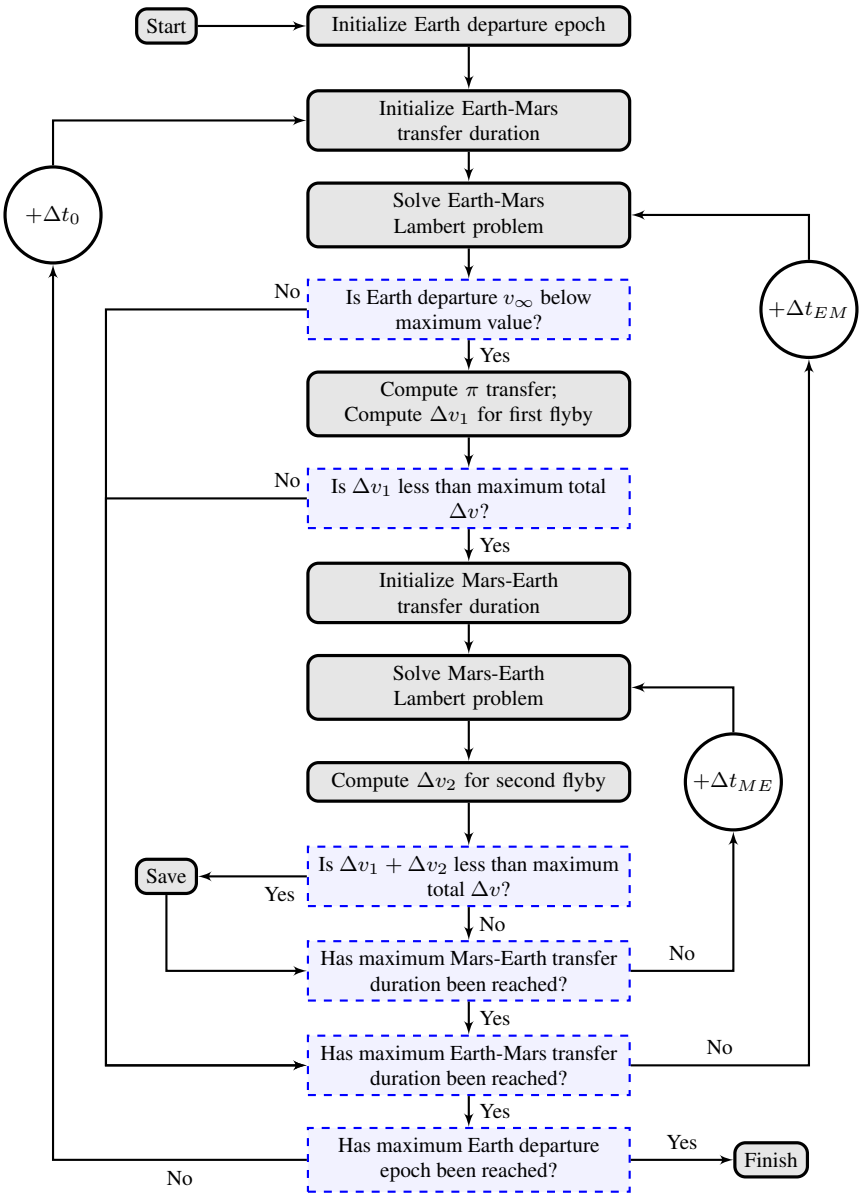

Figure 4. Search algorithm flowchart.

flyby altitude and flyby maneuver magnitude) is written to file. The end result after scanning all possible Earth departure epochs, Earth-Mars transfer durations, and Mars-Earth transfer durations, is a static database which contains all the favorable solutions but which does not contain any unfavorable solutions. A simple search algorithm can then be used to quickly filter out results that do not satisfy additional user-defined constraints. For example, a user could quickly search for all double-flyby free returns that depart Earth in the 2020s and have a flight time under 920 days with an atmospheric entry speed less than 12 km/s. Such a search on the static database requires about 0.1 seconds with the default database resolution used in this study.

RESULTS

The grid search algorithm is used to scan Earth departure dates in the remainder of the century for double-flyby free returns. Each trajectory that requires a total Δv less than 1 m/s is considered a free return and is plotted as a single point in Fig. 5. Beginning in 2022, the ballistic opportunities occur synodically three or four times and then vanish for four synodic periods. This pattern itself repeats about every fifteen years (or, more accurately, every 32 years), the approximate inertial repeat period for Earth and Mars. Figures 6–7 show detailed views of each of the viable launch opportunities. To produce these figures, each launch period was scanned at a finer resolution than the default values given in Table 2. In Figs. 6–7, 'Ballistic' trajectories correspond to double flybys with a total Δv less than 1 m/s, and 'Near-Ballistic' indicates a double flyby with a total Δv between 1 m/s and 10 m/s. These figures show significant variation between opportunities in terms of launch period duration and round trip flight time. It is seen that even though there are some similarities between opportunities, especially at 15 year intervals, it is necessary to perform the scan over a long period of time to capture the valid trajectories at each opportunity. It is incorrect to assume any pattern repeats since the inertial geometry of Earth and Mars never exactly repeats in the ephemeris model. Not shown in Figs. 6–7 are trajectories requiring a total flyby Δv greater than 10 m/s. However, these non-ballistic trajectories may still be useful for double-flyby mission planning since the additional Δv cost may be feasible for certain applications. For missions where such a Δv magnitude is infeasible, these near-ballistic options could become feasible with the addition aerogravity-assist flybys. The flyby Δv of non-free-return trajectories may also be reduced with the inclusion of deterministic deep-space maneuvers. Neither of these topics are considered here, but both are worthy of future study.

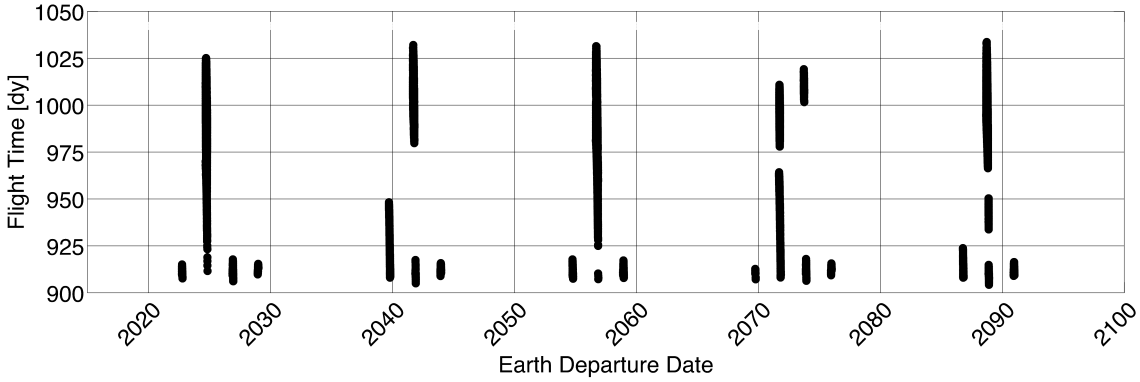

Figure 5. Mars double-flyby free returns (2015–2100).

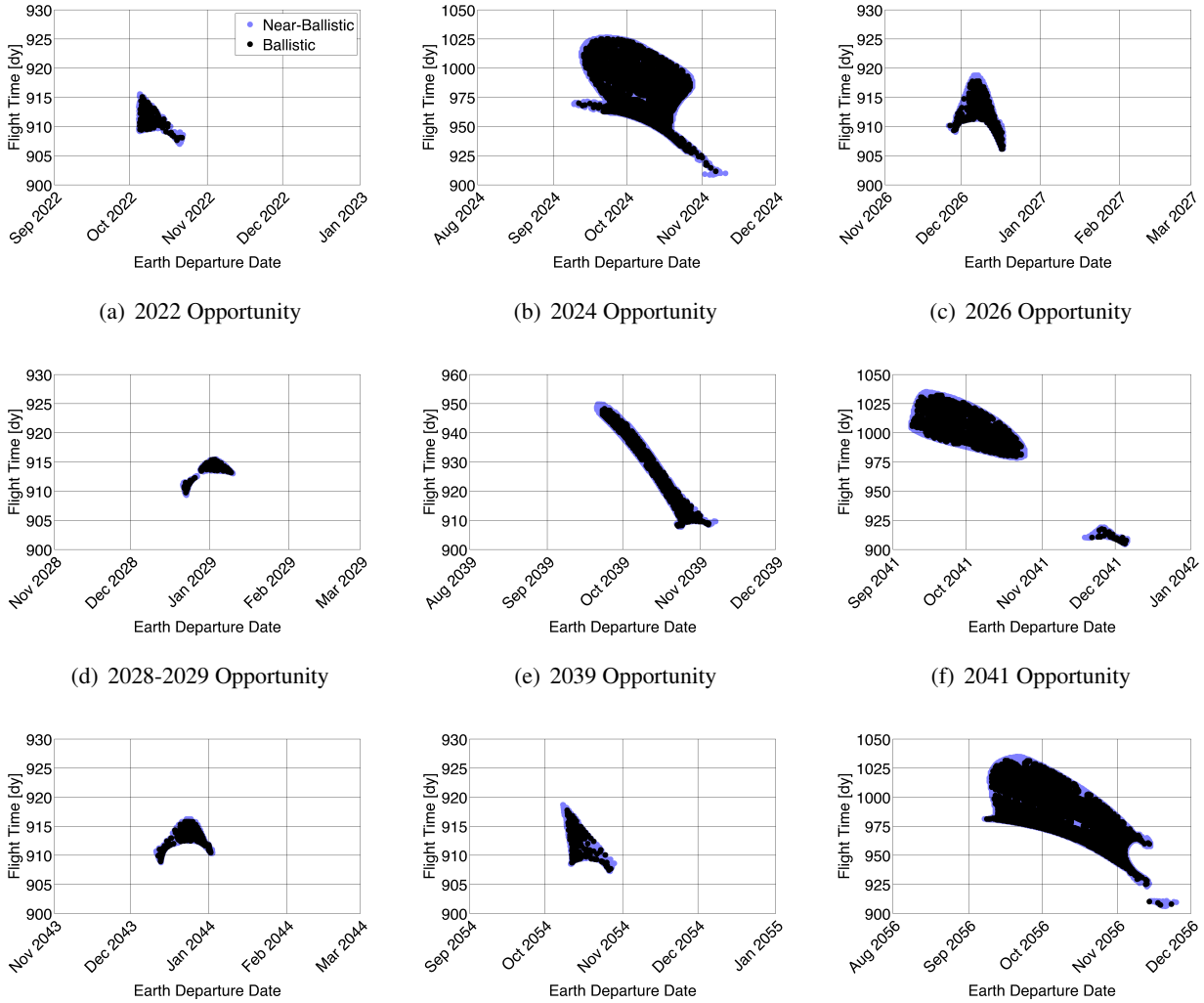

(a) 2022 Opportunity (b) 2024 Opportunity (c) 2026 Opportunity

(d) 2028-2029 Opportunity (e) 2039 Opportunity (f) 2041 Opportunity

(g) 2043-2044 Opportunity (h) 2054 Opportunity (i) 2056 Opportunity

Figure 6. Mars double-flyby free returns (2022–2056).

During the gaps in free-return launch opportunities (for example, before 2022 and between 2029 and 2039), the double-flyby trajectory continues to synodically reach a minimum in total flyby Δv. For example, the best trajectory found in 2020 requires a total flyby Δv of about 215 m/s; ballistic opportunities occur for the following four synodic periods; and the best trajectory in 2031 requires about 275 m/s. Also, the duration of the available launch period for ballistic opportunities is shorter in the boundary years and greater in the interior years of the ballistic groups. For example, the launch period durations in the 2022, 2024, 2026, and 2028-2029 opportunities are 17, 47, 21, and 18 days, respectively. In addition to having the longest launch period and the largest range of possible flight times available in the 2020s, the 2024 opportunity has the minimum Earth departure v_∞ by more than 1 km/s, and the minimum Mars arrival v_∞ by more than 500 m/s.

Tables 3–6 show the free return in each opportunity with the lowest Earth departure energy, lowest Mars arrival energy, shortest flight time, and lowest Earth direct reentry speed, respectively.

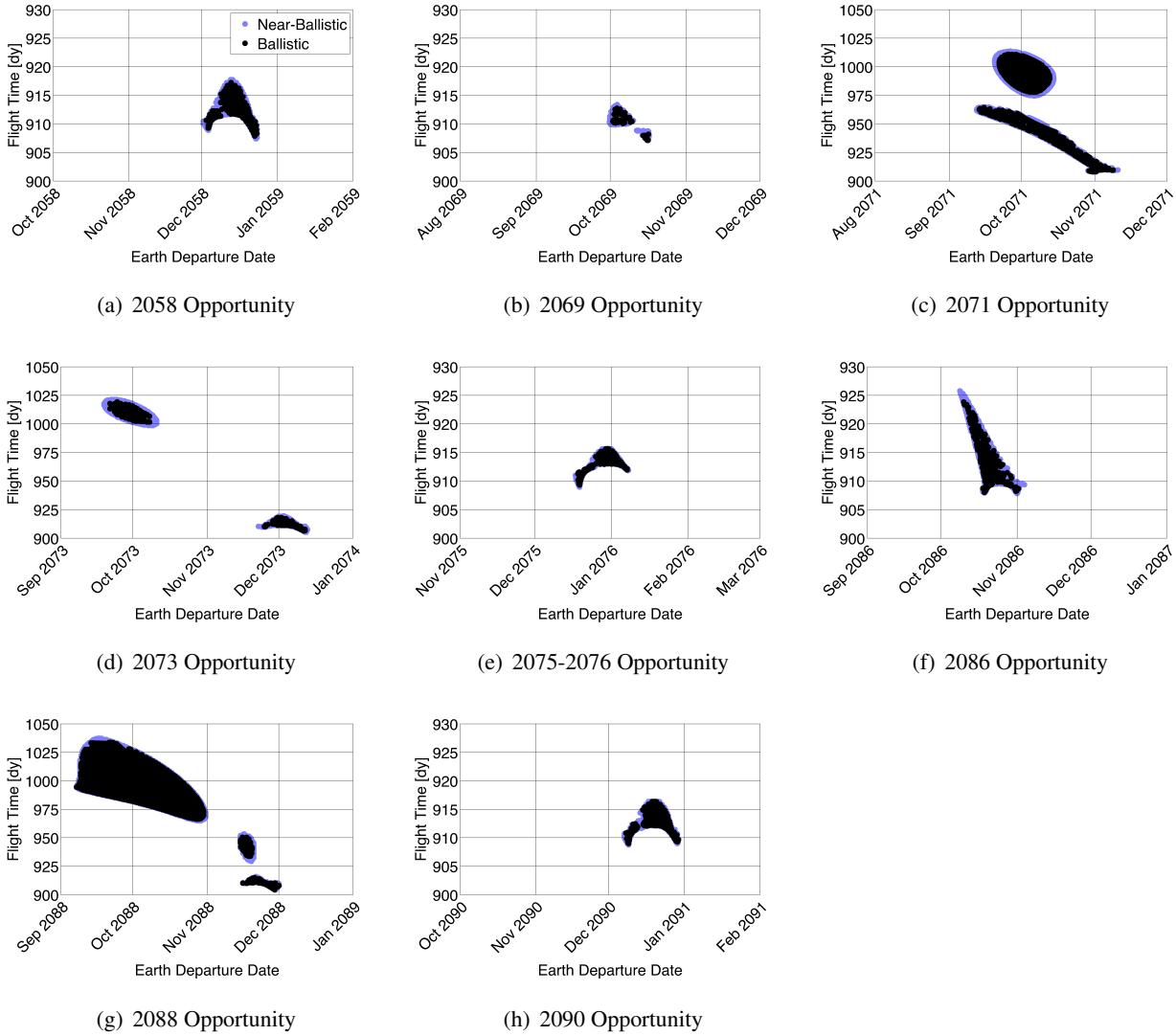

(a) 2058 Opportunity (b) 2069 Opportunity (c) 2071 Opportunity

(d) 2073 Opportunity (e) 2075-2076 Opportunity (f) 2086 Opportunity

(g) 2088 Opportunity (h) 2090 Opportunity

Figure 7. Mars double-flyby free returns (2058–2090).

The launch declination shown in these tables is the angle between the outgoing $\boldsymbol{v}_\infty$ and the Earth's equatorial plane, and the reentry speed calculated here is the hyperbolic periapsis velocity at a radius of 6499 km, an altitude near 125 km. When minimizing a given quantity in a given opportunity, all other quantities were left unconstrained. The overall minimum Earth departure excess speed was found to be 3.155 km/s during the 2041 opportunity. Each of the top five trajectories in this category has a flight time between 970 and 985 days, and an atmospheric reentry speed at Earth under 11.56 km/s. Table 4 shows that the lowest hyperbolic approach speed at Mars in the current scan was found to be 2.566 km/s, which occurs in both 2024 and 2071. In Table 5, the free return with the shortest flight time of 904 days occurs in the 2088 opportunity. This is over 2.5 months shorter than the free return with minimum geocentric departure energy. Relative to the trajectory departing in 2088 with the minimum geocentric energy, the reduced flight time in this case comes at the cost of an increased Earth departure v_∞ of 5.476 km/s, increased flyby speeds at Mars, a

flyby altitude of 200 km (the minimum allowed), and a reentry speed above 11.9 km/s. Table 6 shows that the free return with the overall minimum reentry speed of 11.469 km/s occurs in the 2071 opportunity. The top five opportunities for low reentry speed are the same as the top five for Earth departure energy and Mars approach energy (although in a different order).

Example

Figures 8–9 show an example double-flyby free return, and Table 7 summarizes its itinerary. The trajectory departs Earth on October 10, 2022 with a v_∞ of 4.922 km/s at an equatorial launch declination of 1.4 deg. The outbound leg takes 351 days and approaches Mars with an excess speed of 3.482 km/s (Fig. 8(a)). After the Mars flyby, the trajectory passes above the ecliptic plane and remains above Mars' northern hemisphere during the course of the half-revolution transfer for a duration of about 311 days (Fig. 8(b)). The trajectory's geometry during and near the π transfer provides over 230 days of flight time within one light minute of Mars. At the second flyby, the trajectory has an excess speed of 3.897 km/s, and the return leg from Mars to Earth requires 251 days and results in a direct atmospheric entry speed of 11.837 km/s. No deterministic maneuvers are required after trans-Mars injection; statistical maneuvers will likely be required to correct for unmodeled perturbations and to ensure the proper flyby orientations and to target the Earth atmospheric entry corridor (if a direct entry approach is used). The mission profile is reminiscent of a conjunction-class mission with the key difference being that instead of inserting into orbit around Mars, the trajectory continues in heliocentric orbit and performs a half-revolution transfer back to Mars. Thus, the double-flyby free return takes advantage of Hohmann-like near-minimum energy transfers on the departure and return legs.

Figure 8(c) shows the trajectory viewed along the Mars-Mars axis of the half-revolution transfer. The π transfer is the upper-leftmost segment visible, and the outbound and inbound legs are visible in the bottom right of the figure. From this viewpoint, it is clear that the entire double-flyby free return is nearly planar. This is not surprising, however, since Mars' relatively low mass cannot provide a large flyby turning angle. Figure 9(a) shows the trajectory in a rotating-pulsating reference frame whose principal axis points from Earth to Mars and whose distance unit is scaled by the Earth-Mars distance; the origin is chosen at Earth. This reference frame is also chosen to display the π transfer in Fig. 9(b). This visualization of the half-revolution transfer shows that, from the viewpoint of a Martian observer, the trajectory remains above Mars for the 311 day duration of the π transfer, and, as seen in Fig. 9(c), the relative distance remains within about 0.2 AU for this entire phase. This proximity enables the possibility of enhanced telerobotic surface operations. Figure 9(d) shows the free return's solar distance as a function of flight time. The free return always remains outside of Earth's orbit, and during the half-revolution transfer, the free return's heliocentric distance is nearly the same as that of Mars. This is expected since the first Mars encounter was chosen to produce a post-flyby orbit that was approximately a rotation of Mars' orbit about the sun-Mars line at the flyby epoch.

CONCLUSIONS

Mars double-flyby free returns have been documented through the end of the century with a zero sphere of influence patched conic ephemeris model. This class of free returns offers low energy at Earth departure and return, extensive flight time in near-Mars space, and repeated launch opportunities. Use of the double flyby free return facilitates human and robotic exploration of Mars, including human flyby missions, human surface missions, telerobotic surface operations, robotic

Table 3. Free returns with lowest Earth departure energy during each opportunity

Launch Date, yyyymmdd	Outbound Flight Time, day	Inbound Flight Time, day	Total Flight Time, day	Earth Departure v_∞, km/s	Launch Declination, deg	Mars Arrival v_∞, km/s	Minimum flyby altitude, km	Reentry speed, km/s
20221005	356	248	914	4.533	5.4	3.291	202	11.808
20241005	348	319	972	3.335	21.2	2.568	492	11.493
20261128	309	298	910	4.456	55.0	3.087	231	12.622
20290103	248	363	915	4.391	-18.1	3.901	200	12.099
20390928	371	266	942	3.506	21.7	2.857	234	11.837
20411022	340	343	985	**3.155**	28.6	2.640	249	11.558
20431213	299	303	909	4.379	58.0	3.447	206	12.920
20541009	356	254	918	4.260	12.5	3.120	205	11.805
20561011	346	328	978	3.264	24.5	2.587	922	11.502
20581203	307	300	911	4.402	56.4	3.218	206	12.723
20691003	354	246	913	4.882	-2.2	3.520	203	11.846
20711001	350	324	980	3.409	18.9	2.566	200	11.469
20731008	349	350	1002	3.561	21.9	2.719	200	11.573
20751229	251	361	916	4.366	-12.2	3.742	205	12.044
20861010	359	259	924	3.867	18.6	2.957	200	11.838
20881017	344	338	984	3.203	27.1	2.615	525	11.536
20901209	302	302	909	4.388	57.7	3.339	271	12.849

Table 4. Free returns with lowest Mars arrival energy during each opportunity

Launch Date, yyyymmdd	Outbound Flight Time, day	Inbound Flight Time, day	Total Flight Time, day	Earth Departure v_∞, km/s	Launch Declination, deg	Mars Arrival v_∞, km/s	Minimum flyby altitude, km	Reentry speed, km/s
20221019	312	279	908	6.566	47.4	3.250	217	12.043
20241002	350	323	978	3.346	21.0	**2.566**	503	11.481
20261128	309	298	910	4.456	55.0	3.087	231	12.622
20290105	248	361	915	4.481	-16.9	3.876	204	12.084
20391001	368	266	939	3.515	21.8	2.855	234	11.835
20411022	340	343	985	3.155	28.6	2.640	249	11.558
20431213	299	303	909	4.379	58.0	3.447	206	12.920
20541026	311	283	907	6.340	45.7	3.095	265	12.003
20561013	345	330	978	3.268	24.8	2.585	919	11.502
20581219	259	352	913	5.023	10.7	3.207	218	11.814
20691016	314	274	907	6.746	47.1	3.401	236	12.111
20711001	350	324	980	3.409	18.9	**2.566**	200	11.469
20731008	349	350	1002	3.561	21.9	2.719	200	11.573
20751219	294	306	910	4.431	58.1	3.628	212	12.976
20861010	359	259	924	3.867	18.6	2.957	200	11.838
20881025	336	338	976	3.306	29.7	2.613	346	11.536
20901225	254	358	914	4.840	6.3	3.327	209	11.843

Table 5. Free returns with shortest flight time during each opportunity

Launch Date, yyyymmdd	Outbound flight time, day	Inbound flight time, day	Total Flight Time, day	Earth Departure v_∞, km/s	Launch Declination, deg	Mars Arrival v_∞, km/s	Minimum flyby altitude, km	Reentry speed, km/s
20221019	312	279	908	6.566	47.4	3.250	217	12.043
20241106	319	288	912	4.640	19.9	2.892	338	11.934
20261216	270	334	906	5.433	11.8	3.263	206	11.936
20281222	286	313	910	4.849	61.3	3.930	231	13.073
20391023	324	276	908	5.077	-7.2	3.493	208	12.172
20411205	285	317	905	5.503	15.3	3.174	228	11.945
20431213	299	303	909	4.379	58.0	3.447	206	12.920
20541026	311	283	907	6.340	45.7	3.095	265	12.003
20561118	302	302	907	5.109	21.2	2.909	210	11.918
20581222	265	341	908	5.284	7.6	3.364	219	11.944
20691016	315	273	907	6.792	47.6	3.448	205	12.151
20711030	319	283	908	4.903	-1.2	3.308	231	12.131
20731211	272	332	906	5.482	16.0	3.112	235	11.874
20751219	293	308	909	4.547	59.4	3.667	261	12.995
20861018	331	268	908	4.927	-3.4	3.368	200	12.084
20881129	288	313	**904**	5.476	19.6	3.010	200	11.912
20901209	299	305	909	4.609	60.6	3.409	242	12.870

Table 6. Free returns with lowest Earth reentry speed during each opportunity

Launch Date, yyyymmdd	Outbound flight time, day	Inbound flight time, day	Total Flight Time, day	Earth Departure v_∞, km/s	Launch Declination, deg	Mars Arrival v_∞, km/s	Minimum flyby altitude, km	Reentry speed, km/s
20221006	357	248	915	4.536	6.2	3.300	205	11.789
20240929	353	326	983	3.387	20.7	2.569	487	11.479
20261209	269	345	917	4.869	12.1	3.089	204	11.785
20290105	248	361	915	4.481	-16.9	3.876	204	12.084
20391002	369	270	943	3.519	22.0	2.869	200	11.738
20410916	358	352	1013	4.407	18.8	2.744	451	11.541
20431227	252	360	915	4.546	-0.2	3.461	225	11.902
20541012	354	255	917	4.402	11.4	3.165	207	11.797
20560921	359	335	998	3.776	20.2	2.617	576	11.501
20581217	261	352	915	4.905	9.7	3.208	216	11.814
20691003	354	246	913	4.910	-1.8	3.540	209	11.837
20710929	352	324	982	3.412	19.0	2.566	200	**11.469**
20730923	355	356	1013	4.312	18.6	2.785	212	11.567
20760102	249	362	915	4.470	-8.2	3.655	203	11.981
20861019	348	264	918	4.385	15.4	3.073	203	11.803
20880916	360	345	1008	4.198	19.3	2.691	516	11.524
20901225	254	358	914	4.840	6.3	3.327	209	11.843

Table 7. Example free return timeline

Event	Body	Date, yyyymmdd	Elapsed time, day	Minimum altitude, km	Excess speed, km/s
Departure	Earth	20221010	0	—	4.922
Flyby #1	Mars	20230926	351	291	3.482
Flyby #2	Mars	20240802	662	371	3.897
Arrival	Earth	20250410	913	121	4.177

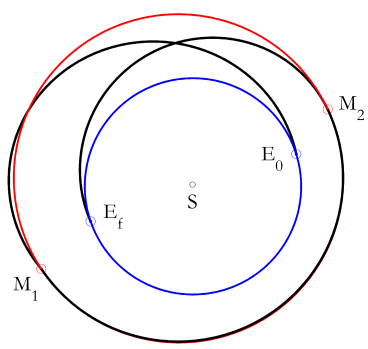

(a) Ecliptic projection

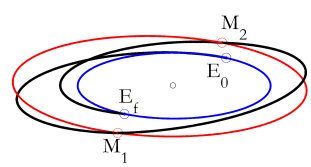

(b) Oblique view

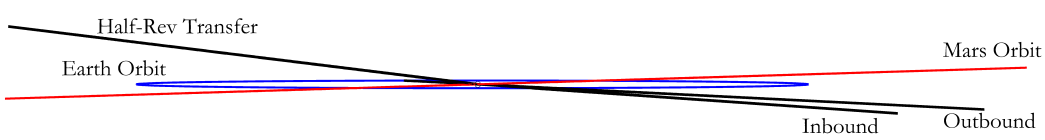

(c) View along Mars-Mars axis of half-revolution transfer

Figure 8. Example Mars double-flyby free return heliocentric visualization. In (a) and (b), E_0 and E_f indicate the initial and final nodes of the free-return at Earth, and M_1 and M_2 indicate the first and second Mars flybys.

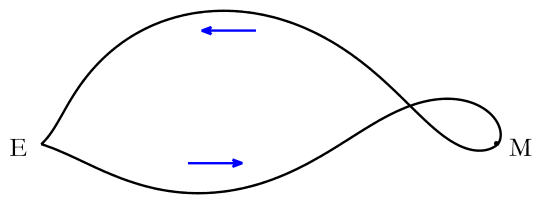

(a) View in rotating-pulsating frame

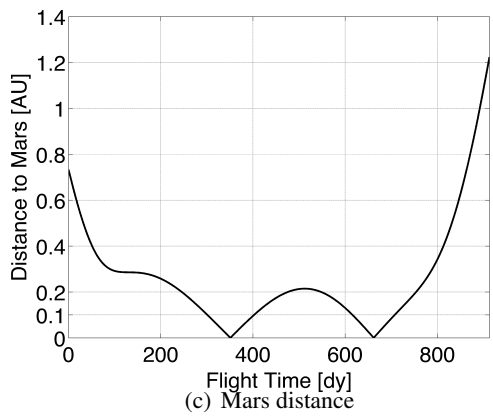

(c) Mars distance

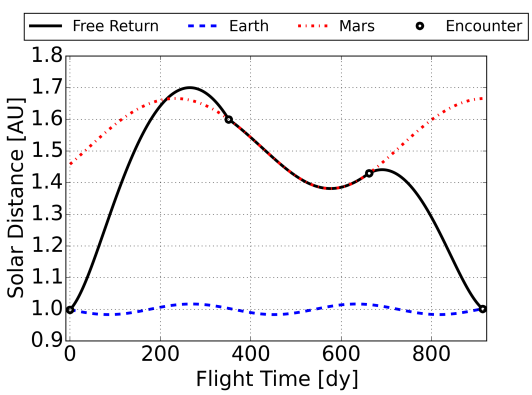

(d) Solar distance

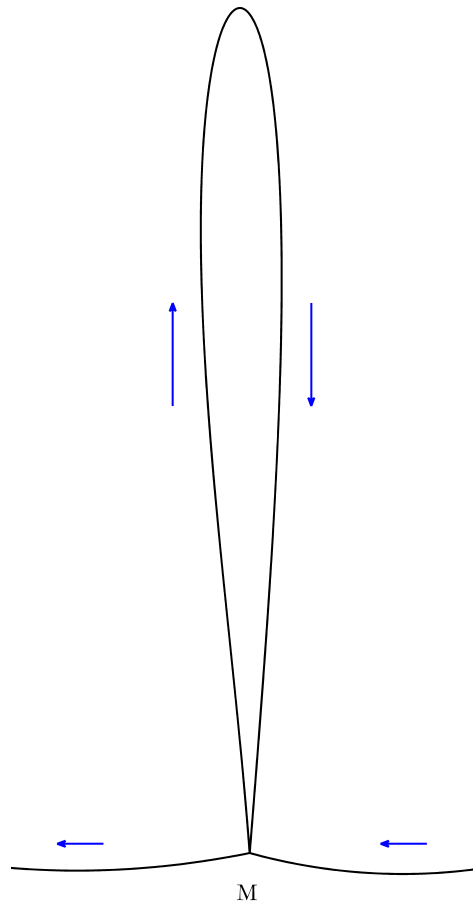

(b) Zoomed view of half-revolution transfer in rotating-pulsating frame

Figure 9. Mars double-flyby free return example.

surface and atmospheric sample return missions, and Phobos/Deimos exploration. For missions that enter the Martian sphere of influence for an extended period, spacecraft components not necessary during this phase may remain on the free return to decrease propellant consumption.

The double-flyby free return requires a trans-Mars injection maneuver similar to conjunction-class trajectories and direct entry speeds within 5% of the those encountered during the Apollo lunar missions. Depending on the injected mass, certain missions may therefore be feasible with current propulsion and entry system technology, but if humans make the journey, advances in deep-space life support systems are required since no double-flyby free return was found with a flight time under 900 days. Some human space travelers have come close to accumulating this total duration in space, but never has this been accomplished in a single flight and never beyond low Earth orbit.

Possible extensions to this work include the analysis of hyperbolic atmospheric passage at Mars for atmospheric sample return missions or in the interest of augmenting the flyby turning angle. Additionally, it will be necessary in future work to transition from the zero sphere of influence ephemeris model to a multibody ephemeris model for more a realistic simulation. Due to the importance of the flyby and reentry geometry to a successful free return mission, it is also critical to understand the statistical uncertainty in the Mars flyby and Earth return states when using a realistic schedule of radiometric tracking data. For viable implementation, it is also necessary to conduct a probabilistic study of trajectory correction maneuvers, since even a "free" trajectory with ballistic Earth return will likely require statistical maneuvers due to, for example, launch injection errors, maneuver execution errors, solar pressure mismodeling, and poorly-modeled perturbations like spacecraft outgassing. Such research will deepen the understanding of the double-flyby free return for flight applications.

With over 20 successful robotic missions to Mars and over 40 attempts, and with sustained interest in human missions, the Red Planet remains a prime target for exploration. Evidence of surface water in Mars' past allows the possibility of extinct or extant life, which also makes Mars a prime scientific target. And with water ice and abundant carbon dioxide, Mars may be the next world for human colonization. The double flyby free return trajectory is a viable option to support these endeavors.

ACKNOWLEDGMENTS

This research was carried out at the Jet Propulsion Laboratory, California Institute of Technology, under a contract with the National Aeronautics and Space Administration. I thank Tomas Martin-Mur, Juan Arrieta, Juan Senent, and Anastassios Petropoulos for their helpful discussions on this topic.

REFERENCES

[1] R. Zubrin, "Athena - A Potential First Step in a Program of Human Mars Exploration," *AIAA Space Programs and Technologies Conference*, AIAA Paper 96-4465, Sept. 1996.

[2] E. C. Lineberry and J. K. Soldner, "Mission Profiles for Human Mars Missions," *AIAA Space Programs and Technologies*, AIAA Paper 90-3794, Sept. 1990.

[3] R. W. Orloff, *Apollo by the Numbers: A Statistical Reference*, pp. 276,291,305. Washington: U. S. Government Printing Office, 2000.

[4] R. R. Titus, "FLEM - Flyby-Landing Excursion Mode," *3rd Aerospace Sciences Meeting*, AIAA Paper 66-36, Jan. 1966.

[5] A. A. Wolf, "Free Return Trajectories for Mars Missions," *AAS/AIAA Space Flight Mechanics Meeting*, AAS Paper 91-123, Feb. 1991.

[6] M. R. Patel, J. M. Longuski, and J. A. Sims, "Mars Free Return Trajectories," *Journal of Spacecraft and Rockets*, Vol. 35, No. 3, 1998, pp. 350–354.

[7] T. Crain, R. H. Bishop, and W. Fowler, "Interplanetary Flyby Mission Optimization Using a Hybrid Global-Local Search Method," *Journal of Spacecraft and Rockets*, Vol. 37, No. 4, 2000, pp. 468–474.

[8] E. P. Bonfiglio, J. M. Longuski, and N. X. Vinh, "Automated Design of Aerogravity-Assist Trajectories," *Journal of Spacecraft and Rockets*, Vol. 37, No. 6, 2000, pp. 768–775.

[9] M. Okutsu and J. M. Longuski, "Mars Free Returns via Gravity Assist from Venus," *Journal of Spacecraft and Rockets*, Vol. 39, No. 1, 2002, pp. 31–36.

[10] C. S. Rall, "Free-Fall Periodic Orbits Connecting Earth and Mars," *AIAA Aerospace Sciences Meeting*, New York, NY, AIAA Paper 71-92, Jan. 1971.

[11] D. V. Byrnes, J. M. Longuski, and B. Aldrin, "Cycler Orbit Between Earth and Mars," *Journal of Spacecraft and Rockets*, Vol. 30, No. 3, 1993, pp. 334–336.

[12] T. T. McConaghy, D. F. Landau, C. H. Yam, and J. M. Longuski, "Notable Two-Synodic-Period Earth-Mars Cycler," *Journal of Spacecraft and Rockets*, Vol. 43, No. 2, 2006, pp. 456–465.

[13] R. P. Russell and C. A. Ocampo, "Optimization of a Broad Class of Ephemeris Earth-Mars Cyclers," *Journal of Guidance, Control, and Dynamics*, Vol. 29, No. 2, 2006, pp. 354–367.

[14] W. V. Braun, *The Mars Project*. University of Illinois Press, 1953.

[15] S. C. Himmel, J. F. Dugan Jr, R. W. Luidens, and R. J. Weber, "A Study of Manned Nuclear-Rocket Missions to Mars," *Aerospace Engineering*, Vol. 20, No. 7, 1961, pp. 18–58.

[16] A. Cohen, *Report of the 90-Day Study on Human Exploration of the Moon and Mars*. National Aeronautics and Space Administration, 1989.

[17] R. M. Zubrin and D. A. Baker, "Mars Direct: Humans to the Red Planet by 1999," *Acta Astronautica*, Vol. 26, No. 12, 1992, pp. 899–912.

[18] R. M. Zubrin and D. B. Weaver, "Practical Methods for Near-Term Piloted Mars Missions," *AIAA/SAE/ASME/ASEE Joint Propulsion Conference & Exhibit*, AIAA Paper 93-2089, June 1993.

[19] S. J. Hoffman and D. L. Kaplan, "Human Exploration of Mars: The Reference Mission of the NASA Mars Exploration Study Team," NASA SP 6107, July 1997.

[20] B. G. Drake, "Reference Mission Version 3.0, Addendum to the Human Exploration of Mars: The Reference Mission of the NASA Mars Exploration Study Team," NASA EX13-98-036, June 1998.

[21] B. G. Drake, "Human Exploration of Mars: Design Reference Architecture 5.0," NASA SP-2009-566, July 2009.

[22] J. P. Grotzinger, J. Crisp, A. R. Vasavada, R. C. Anderson, C. J. Baker, R. Barry, *et al.*, "Mars Science Laboratory Mission and Science Investigation," *Space Science Reviews*, Vol. 170, No. 1–4, 2012, pp. 483–486.

[23] F. P. Dixon, "The EMPIRE Dual Planet Flyby Mission," *Engineering Problems of Manned Interplanetary Exploration*, 1963.

[24] R. R. Titus, "Powered Flybys of Mars," *AIAA Second Annual Meeting*, AIAA Paper 65-515, July 1965.

[25] R. R. Titus, "Early Manned Exploration of the Planets," *Journal of Spacecraft and Rockets*, Vol. 8, No. 5, 1971, pp. 517–522.

[26] N. R. Augustine, W. M. Austin, C. Chyba, C. F. Kennel, B. I. Bejmuk, E. F. Crawley, *et al.*, "Seeking a Human Spaceflight Program Worthy of a Great Nation," Review of U.S. Human Spaceflight Plans Committee, Oct. 2009.

[27] D. A. Tito, G. Anderson, J. P. Carrico, J. Clark, B. Finger, G. A. Lantz, *et al.*, "Feasibility Analysis for a Manned Mars Free-Return Mission in 2018," *IEEE Aerospace Conference*, Mar. 2013.

[28] D. M. Hassler, C. Zeitlin, R. F. Wimmer-Schweingruber, B. Ehresmann, S. Rafkin, J. L. Eigenbrode, *et al.*, "Mars Surface Radiation Environment Measured with the Mars Science Laboratory's Curiosity Rover," *Science*, Vol. 343, No. 6169, 2014, p. 1244797.

[29] P. N. Desai and G. D. Qualls, "Stardust Entry Reconstruction," *Journal of Spacecraft and Rockets*, Vol. 47, No. 5, 2010, pp. 736–740.

[30] C. H. Acton, "Ancillary Data Services of NASA's Navigation and Ancillary Information Facility," *Planetary and Space Science*, Vol. 44, No. 1, 1996, pp. 65–70.